Materials Advances

ROYAL SOCIETY OF CHEMISTRY

PAPER

View Article Online
View Journal | View Issue

Cite this: *Mater. Adv.*, 2020, **1**, 1455

A microporous, amino acid functionalized Zn(II)-organic framework nanoflower for selective CO_2 capture and solvent encapsulation†

Shradha Gandhi, Prasenjit Das and Sanjay K. Mandal *

A new homochiral metal organic framework, $\{[Zn_4(\mu_3\text{-}OH)_2(D\text{-}2,4\text{-}cbs)_2(H_2O)_4]\cdot 5H_2O\}_n$ (**Zn-CBS**), has been solvothermally synthesized using a new chiral amino acid based tricarboxylic acid ligand, (2-((4-carboxybenzyl)amino)succinic acid), H_3(D-2,4-cbs). **Zn-CBS** was characterized by various techniques like Fourier transform infrared spectroscopy (FTIR), UV-Vis solid-state diffuse reflectance spectroscopy, elemental microanalysis, thermogravimetric analysis (TGA), powder X-ray diffraction (PXRD), field emission scanning electron microscopy (FESEM), high resolution transmission electron microscopy (HRTEM), and energy dispersive X-ray analysis (EDX) and elemental mapping. The nanoflower arrangement in **Zn-CBS** is clearly seen from the FESEM and TEM images. Its microporous nature is established by the nitrogen adsorption measurements which exhibit a reversible type I isotherm with a BET surface area of 282 $m^2\ g^{-1}$. Similarly, it shows a reversible type I isotherm for H_2 with an uptake of 0.5 wt% at 77 K. Based on its CO_2 sorption isotherm with an uptake of 85.9 $cm^3\ g^{-1}$ at 195 K, a high isosteric heat of adsorption (Q_{st}) of 35 kJ mol^{-1} at zero coverage is obtained. This is illustrated by its high potential of selectivity towards CO_2 over N_2 and CH_4 under ambient conditions (298 K and 1 bar). With the help of configurational bias Monte Carlo molecular simulation, this selectivity is explained for an effective interaction between CO_2 and basic amine sites of the framework. The porous nature and functionality of **Zn-CBS** have also been utilized in encapsulating various small molecules, which is followed by FTIR, TGA and PXRD.

Received 6th July 2020,
Accepted 20th July 2020

DOI: 10.1039/d0ma00481b

rsc.li/materials-advances

Introduction

In the past couple of decades, there has been growing interest in the study of Metal–Organic Frameworks (MOFs), made from a combination of suitable organic ligands and metal ions, owing to their highly porous nature with structural diversity, tunable functionality and large surface area. These properties play vital roles in various applications, such as gas and vapour adsorption, catalysis, sensing, magnetism, *etc.*[1–12] In particular, their promising roles in carbon capture have received significant attention for an urgent need to reduce the concentration of the major greenhouse gas CO_2 as it is a part of flue gases which has a toxic effect on the environment.[13] Also, the composition of landfill gas has CO_2 along with CH_4 (CO_2/CH_4 = 50/50) that needs to be separated out, which is essential for natural gas purification.[14–16] As the landfill-gas is a combination of polar (CO_2) and non-polar (CH_4) gas, the criteria for the selectivity of CO_2 are: (a) an access to open metal sites and polar N-containing basic functional groups, which show adsorbate–adsorbent interaction due to quadrupole interaction of CO_2 molecules with the framework,[14–32] and (b) an appropriate pore diameter of the framework for size/shape exclusion.[31–36] It should be noted that initial efforts with zeolitic and zeolitic-like metal imidazolate framworks (ZIFs) that have excellent affinity for CO_2 due to the presence of –N(H) donors on the imidazole moieties have suffered for less uptake capacity and selectivity for CO_2 for not having open metal sites.[37] On the other hand, flue gases also have water vapour apart from CO_2. Thus, the framework ought to eliminate water vapor alongside the greenhouse gas. To make an MOF potential for H_2O adsorption, it must be water stable and shows very good interaction with water. Among robust water and thermally stable MOF materials, those with the well-known Zn_4O core appeared to be desirable.[38] Interestingly, a limited number of MOFs with the $Zn_4(\mu_3\text{-}OH)_2$ core has been reported; moreover, those with trianionic linkers such as benzene tricarboxylate (BTC) and 2-sulfoterephthalate (STP) are rare.[25,39]

Department of Chemical Sciences, Indian Institute of Science Education and Research Mohali, Sector 81, Manauli PO, S.A.S. Nagar, Mohali, Punjab 140306, India. E-mail: sanjaymandal@iisermohali.ac.in

† Electronic supplementary information (ESI) available: Scheme S1, Fig. S1–S21 and Tables S1–S4. Synthesis and characterization of H_3(D-2,4-cbs) and Zn-CBS; sorption isotherms; comparison of data with literature. See DOI: 10.1039/d0ma00481b

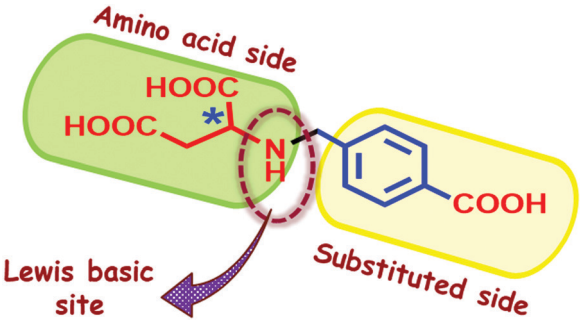

Fig. 1 Structure of H_3(D-2,4-cbs) ligand.

With the above considerations, we chose to explore the use of amino acid functionalized tricarboxylates to synthesize MOFs with the $Zn_4(\mu_3\text{-}OH)_2$ core that will offer (a) to contain –N(H) functional groups and open metal sites, and (b) to tailor pore sizes by varying the aldehyde used in making the tricarboxylate. We believe that our approach is simple and cost-effective to introduce multiple functionalities into the MOFs.[40–43] Furthermore, the presence of amino acid in the system also provides an opportunity to add chirality in the MOFs.[44] Whereas, if the framework is found to be microporous in nature it will be suitable for hydrogen sorption.[45,46] Thus, we targeted to make a microporous MOF using one of the two amino acids that have two carboxylic acid groups (aspartic acid and glutamic acid) and functionalize their amine part with 4-formyl benzoic acid through the reduced Schiff base chemistry to demonstrate our concept.

Herein, we have synthesized a new chiral ligand (2-((4-carboxybenzyl)amino)succinic acid) H_3(D-2,4-cbs) with one secondary amine group and three carboxylic acid group (Fig. 1) from very cheap D-aspartic acid. Using this ligand, a microporous and versatile MOF, $\{[Zn_4(\mu_3\text{-}OH)_2(D\text{-}2,4\text{-}cbs)_2(H_2O)_4]\cdot 5H_2O\}_n$ **(Zn-CBS)**, has been solvothermally synthesized and characterized by various analytical techniques. The basic functionality present on the pore wall is utilized for selective CO_2 capture and separation over N_2 (flue gas) and CH_4 (landfill gas). Along with CO_2, **Zn-CBS** also shows smart adsorption behavior towards H_2. Furthermore, its water vapour sorption isotherm illustrates steep uptake behavior at low relative pressure. **Zn-CBS** is also found to be efficient in encapsulating solvent molecules.

Experimental section

Materials and methods

All chemicals and solvents used for synthesis were obtained from Sigma-Aldrich and Merck and were used as received, without further purification. All reactions were carried out under aerobic conditions.

Physical measurements

Using samples prepared as KBr pellets, Fourier transform infrared (FTIR) spectra were measured in the 4000–400 cm^{-1} range on a PerkinElmer Spectrum I spectrometer. For melting point determination, a Büchi M-565 instrument was used. Solid-state diffuse reflectance spectra were recorded using a Cary 5000 UV-vis-NIR instrument by Agilent Technology. The ^1H NMR spectra were recorded on a Bruker ARX-400 spectrometer in D_2O at 25 °C. Thermogravimetric analysis (TGA) were carried out from 30 to 500 °C (at a heating rate of 10 °C min^{-1}) under a dinitrogen atmosphere using a Shimadzu DTG-60H instrument. High Resolution Mass Spectrometry (HRMS) data were measured by Thermo Scientific LTQ XL LC-MS instrument for the 50–2000 amu range with ESI,† ion source. Powder X-ray diffraction (PXRD) measurements were done on a Rigaku Ultima IV diffractometer equipped with a 3 kW sealed tube Cu Kα X-ray radiation and a DTex Ultra detector using Bragg–Brentano beam geometry over a 2θ range from 5 to 40° with a scan speed of 2° per min and 0.02° step width. Wide angle X-ray (WAX) measurements were carried out using Xeuss Model C HP100 fm from Xenocs. Scattering vector ($q = 4\pi\sin\theta/\lambda$) and position of an incident X-ray beam on the detector were calibrated using several orders of layer reflections from silver behenate while scattering and diffraction images were recorded and integrated along the Debye–Scherrer ring using the FIT2D software. Field emission scanning electron microscopy (FESEM) experiments, including energy dispersive X-ray spectroscopy (EDX) for mapping of elements, were performed on a JEOL instrument; each sample was well dispersed in ethanol, drop casted on a silicon wafer, dried and coated with gold using a working distance of 4.5–15 mm and a voltage of 10–15 kV. High-resolution transmission electron microscopy (HRTEM) was performed on a FEI Tecnai G2 F20 equipped with a field emission gun operated at 200 kV using a copper grid loaded with the dispersed sample (1 mg in 10 mL ethanol sonicated for 20 min) followed by drying with a lamp for 30 minutes. Gas sorption experiments were performed using a BELSORP MAX (BEL JAPAN) volumetric adsorption analyzer at different temperatures. Ultrapure (99.995%) N_2, He, H_2, CH_4 and CO_2 gases were used for the adsorption measurements. Prior to the adsorption measurement, the sample was ground into a fine powder, evacuated at 393 K for 24 h and purged with ultrapure nitrogen gas on cooling.

Synthesis of 2-((4-carboxybenzyl)amino)succinic acid [H_3(D-2,4-cbs)]

In a 50 mL round bottom flask, D-aspartic acid (106.4 mg, 0.8 mmol) and NaOH (64 mg, 1.6 mmol) were dissolved in 20 mL dry methanol and stirred for half an hour at 25 °C. To the resulting mixture, 4-formyl benzoic acid (120 mg, 0.8 mmol) was added and stirred for 4 h to get a colorless solution that was cooled using an ice bath for the next step. Upon addition of solid $NaBH_4$ (60.48 mg, 0.62 mmol), the reaction mixture was stirred for another 8 h. After removal of methanol under reduced pressure, the obtained residue was dissolved in water and the pH was adjusted to 4–5 by adding acetic acid, which resulted in the precipitation of a white solid. The solid was isolated by filtration, thoroughly washed with water, and dried under vacuum. Yield: 124 mg (60%). M.P. 243 °C. HRMS (ESI) *m/z*: cal. $[M + H]^+$: 268.058, found: 268.057. ^1H NMR (D_2O, 400 MHz): δ 2.1 (m, 2H), 3.2 (dd, 1H), 3.5 (m, 2H), 7.2 (d, 2H),

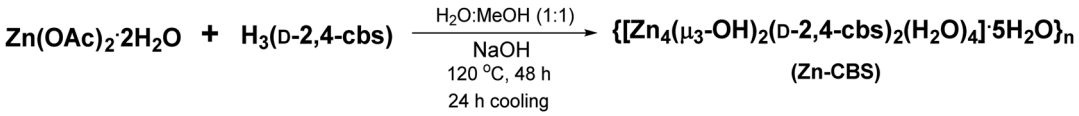

Scheme 1 Solvothermal synthesis of **Zn-CBS**.

7.6 (d, 2H) ppm. Selected FTIR peaks (KBr pellet, cm^{-1}): 2969 (br), 1691 (s), 1618 (s), 1429 (m), 1299 (m), 1189 (m), 750 (m).

Synthesis of $\{[Zn_4(\mu_3\text{-}OH)_2(D\text{-}2,4\text{-}cbs)_2(H_2O)_4]\cdot 5H_2O\}_n$ (Zn-CBS)

A mixture of $Zn(OAc)_2\cdot 2H_2O$ (32 mg, 0.11 mmol), NaOH (8.88 mg, 0.22 mmol) and H_3(D-2,4-cbs) (20 mg, 0.074 mmol) in MeOH/H_2O (1 mL/1 mL) was heated in a 10 mL capacity Teflon lined stainless-steel reactor at 120 °C for 48 h and then cooled to room temperature in 24 h. A white precipitate that was formed was collected by filtration, washed with acetonitrile/toluene and dried in air. Yield: 19 mg (54%). Anal. Calc. (%) for $C_{24}H_{40}N_2O_{23}Zn_4$ (MW 986.09): C, 27.5; H, 3.79; N, 2.92. Found: C, 27.8; H, 3.40; N, 2.5. Selected FTIR peaks (KBr pellet, cm^{-1}): 3421 (br), 3239 (br), 1617 (s), 1398 (s),1099 (w), 1010 (w), 882 (w).

Results and discussion

Synthesis and characterization

The chiral ligand H_3(D-2,4-cbs) used in this study was prepared from D-aspartic acid, which was first converted to its disodium salt, and 4-formylbenzaldehyde in a single pot using the standard Schiff base chemistry in dry methanol followed by reduction with sodium borohydride (Scheme S1, ESI†). Its isolation as a solid was aided by the addition of glacial acetic acid to the reduced Schiff base obtained in the second step. This ligand was characterized by FTIR, TGA, HRMS, and NMR spectroscopy (Fig. S1–S4, ESI†). For the synthesis of **Zn-CBS**, a solvothermal reaction of $Zn(OAc)_2\cdot 2H_2O$, NaOH and H_3(D-2,4-cbs) was carried out in a mixture of methanol and water at 120 °C for 48 h followed by cooling to room temperature in 24 h with an yield of 54% (Scheme 1). Several attempts to obtain suitable single crystals of **Zn-CBS** for the X-ray study were not successful. However, in addition to the extensive characterization by elemental analysis, spectroscopic and microscopic analysis, the crystallinity and phase purity as well as thermal stability of **Zn-CBS** were studied by in-situ PXRD and TGA for its applications. These are discussed in detail below.

In the FTIR spectrum of **Zn-CBS**, the presence of water molecules and the OH groups within the core is substantiated by the observation of a strong peak at 3421 cm^{-1}. Similarly, a broad peak at 3239 cm^{-1} corresponds to the –NH group from the ligand (Fig. S5, ESI†).[47] The asymmetric and symmetric stretching frequencies for the carboxylate appears at 1622 cm^{-1} and 1397 cm^{-1}, respectively, with a difference of 225 cm^{-1}, which corresponds to the monodentate binding mode of the carboxylate groups.[47] The solid-state diffuse reflectance spectrum of **Zn-CBS** exhibited two peaks at 245 and 280 nm attributed to the ligand-based π–π* transitions (Fig. S6, ESI†).

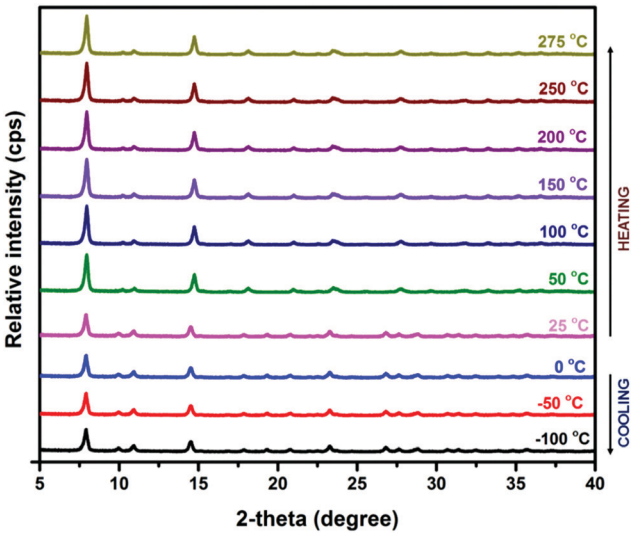

Fig. 2 Variable temperature PXRD patterns of **Zn-CBS**.

Thermochemistry by TGA and VT-PXRD

To examine the thermal stability of **Zn-CBS**, the TG experiment was carried out from 30 °C to 500 °C under a nitrogen atmosphere. In the first step of its TG profile, a weight loss of 9.5% (calc. 9.3%) corresponding to five lattice water molecules is observed between 30 °C to 80 °C (Fig. S7, ESI†). Thereafter, it is stable up to 275 °C followed by decomposition.

The purity and crystallinity of **Zn-CBS** at room temperature was evaluated by PXRD (Fig. S8, ESI†) and further confirmed by the 2D WAX map (Fig. S9, ESI†). Based on the thermal stability of the framework shown by TGA, **Zn-CBS** was investigated by in-situ VTPXRD to provide insight into their crystalline properties at different temperatures (from −100 °C to 275 °C). As shown in Fig. 2, it maintains the structure and crystallinity throughout the cooling and heating cycles. The high crystallinity and stability of **Zn-CBS** up to 275 °C can be due to the formation of a stable $[Zn_4(\mu_3\text{-}OH)_2]$ core in its 3D structure.[39]

Surface analysis

To figure out the morphology of **Zn-CBS**, both FESEM and TEM were utilized. Its FESEM image (Fig. 3a) shows accumulation and assembling of leaves to form nanoflowers, which indicate the chiral nature of the framework.[48] The morphology is further confirmed by TEM showing aggregation of leaflets (Fig. 3b). Moreover, the TEM image shows that the size of the leaflet is in the range of 79–90 nm. The HRTEM image shows well-defined lattice fringes with spacing of 0.23 nm for the nanoflowers (Fig. 3c). Its compositional characterization was done by EDX and elemental mapping (Fig. 3d, e and Fig. S10, ESI†), where

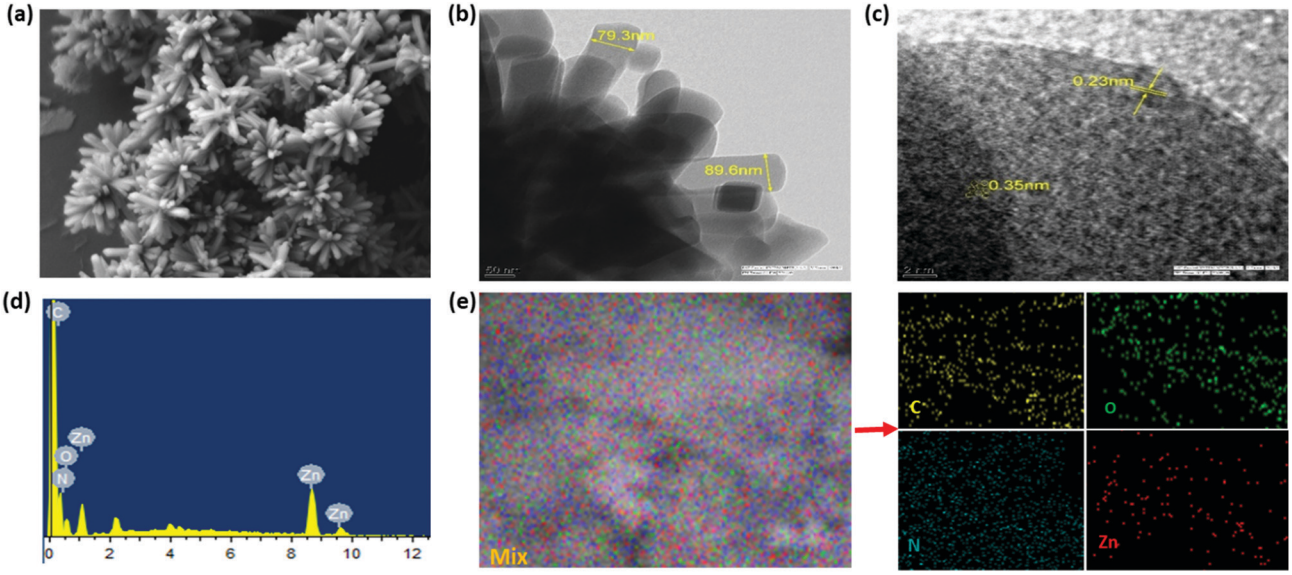

Fig. 3 Characterization of **Zn-CBS**: (a) FESEM image showing nanoflower morphology; (b) TEM image showing accumulation of leaflets; (c) HRTEM image; (d) EDX spectrum; and (e) elemental mapping.

peaks for Zn, O, N and C were observed. In particular, the % of Zn was found to be very close to the theoretical value for **Zn-CBS**.

Gas and vapor sorption study

The microporous nature of **Zn-CBS** is utilized for significant adsorption towards gas (N_2, H_2, CO_2, and CH_4), and vapor (H_2O). For adsorption measurements, each time the compound was activated at 120 °C for 24 h under high vacuum. To evaluate its porosity, N_2 sorption isotherm at 77 K has been measured and evaluated. It exhibits a reversible type I isotherm with a pore diameter of 0.6 nm, signifying microporous nature of the framework (Fig. 4a). With a maximum N_2 uptake of 106.98 $cm^3\ g^{-1}$ at 1 atm, Langmuir and Brunauer–Emmett–Teller (BET) surface areas are calculated to be 350.21 and 282 $m^2\ g^{-1}$, respectively. For its microporous nature, the adsorption of H_2 with an uptake of 64 $cm^3\ g^{-1}$ (STP) was observed as shown in Fig. 4b. Its uptake of H_2 (0.5 wt%) is comparable and higher than $[Zn_2(tcpcdp)]$ (0.2 wt%),[14] $[Zn_4O(adc)_3]$ (0.4 wt%),[30] $[Zn_2(btatb)(EtPy)]$ (0.57 wt%),[23] and $[Zn_2(btatb)(MePy)]$ (0.59 wt%).[16]

The kinetic diameters of CO_2 and CH_4 are 3.3 Å and 3.8 Å, respectively, which are suitable for the pore of **Zn-CBS** to adsorb both the gases. The CO_2 sorption isotherms were measured at 195 K, 263 K, 273 K, and 298 K (0–1.0 atm) depicting typical type I isotherm. At 298 K, 273 K, 263 K and 195 K, the uptake amounts of CO_2 are 38.7 $cm^3\ g^{-1}$ (STP; 7.6 wt%), 47.5 $cm^3\ g^{-1}$ (STP; 9.3 wt%), 49.3 $cm^3\ g^{-1}$ (STP; 9.6 wt%) and 85.9 $cm^3\ g^{-1}$ (STP; 16.8 wt%), respectively (Fig. 4c). Interestingly, its uptake of CO_2 is higher or comparable with other amine or amino acid based system (Table S1, ESI†).[12,19] On the other hand, the uptake of CH_4 is less compared to CO_2 at 298 K, 273 K, and 263 K, which are 15.1 $cm^3\ g^{-1}$, 21.2 $cm^3\ g^{-1}$, and 24.8 $cm^3\ g^{-1}$, respectively (Fig. 4d). However, **Zn-CBS** shows higher value for CH_4 than SNU-77S, SNU-100, SNU-150 and SNU-151,[16–41] IITKGP-5 and IITKGP-6,[15,29] $[Zn_2(BDC)_2(DABCO)_2]$[23] (Table S1, ESI†). For comparison, the N_2 uptake amounts are 4.1 $cm^3\ g^{-1}$ at 298 K, 6.6 $cm^3\ g^{-1}$ at 273 K and 8.1 $cm^3\ g^{-1}$ at 263 K (Fig. S11, ESI†). The high uptake of CO_2 over N_2 and CH_4 reflect very strong dipole–quadrupole interaction between CO_2 molecules and the amine-functionalized pore wall of **Zn-CBS**.

The interaction between the framework and gas molecules is calculated by isosteric heat of adsorption (Q_{st}) by the Clausius–Clapeyron equation at 263 K, 273 K, and 298 K. The values for CO_2, CH_4 and N_2 at zero coverage are 35 kJ mol^{-1}, 51.8 kJ mol^{-1} and 0.7 kJ mol^{-1}, respectively (Fig. 5). It is important to note that the Q_{st} of CH_4 is remarkably higher compared to CO_2. These Q_{st} values have been compared with other MOFs (Table S1, ESI†). Interestingly, **Zn-CBS** shows comparable and higher Q_{st} for CO_2 than MIL-53(Cr) (32 kJ mol^{-1}),[20] IRMOF-9-NMe_2 (27 kJ mol^{-1}),[21] TEA@bio-MOF-1 (26.5 kJ mol^{-1}),[22] CPF-13 (28.3 kJ mol^{-1}),[14] JUC-141 (27.85 kJ mol^{-1}),[10] IISERP-MOF20 (26 kJ mol^{-1}),[12] $[Zn(atz)_2]$ (26 kJ mol^{-1}),[16] $[Zn_2(BDC)_2(DABCO)]$ (25 kJ mol^{-1}),[23] NOTT-202a (22 kJ mol^{-1}),[24] $[Zn_4(OH)_2(1,2,4\text{-}BTC)_2]$ (20 kJ mol^{-1}),[25] and IRMOF-3 (19 kJ mol^{-1}).[26] Whereas, the Q_{st} for methane is higher than those reported for the MOFs in the literature, such as, SNU-100 (26.5 kJ mol^{-1}),[16] JUC-141 (22.7 kJ mol^{-1}),[10] $[Zn(atz)_2]$ (19.5 kJ mol^{-1}),[16] IITKGP-6 (18.4 kJ mol^{-1}),[29] SNU-151 (18.2 kJ mol^{-1}),[41] IITKGP-5 (14.8 kJ mol^{-1}),[15] SNU-77S (14.3 kJ mol^{-1}),[41] and SNU-150 (12.8 kJ mol^{-1}).[41]

Motivated by the polar functional pore surface, the water sorption isotherm of **Zn-CBS** has been measured to check its stability in water. It shows a type I isotherm with high H_2O uptake of ~156 cm^3 (STP) g^{-1} at lower P/P_0 values (at 0.2), amounting to five water molecules per formula unit. This corroborates well with its microanalysis where five lattice water molecules have been determined. Its sorption and desorption curves properly overlap, indicating no hysteresis loop for retaining any water molecules inside the pore upon desorption. Its ability for a large water uptake at low pressure and a long

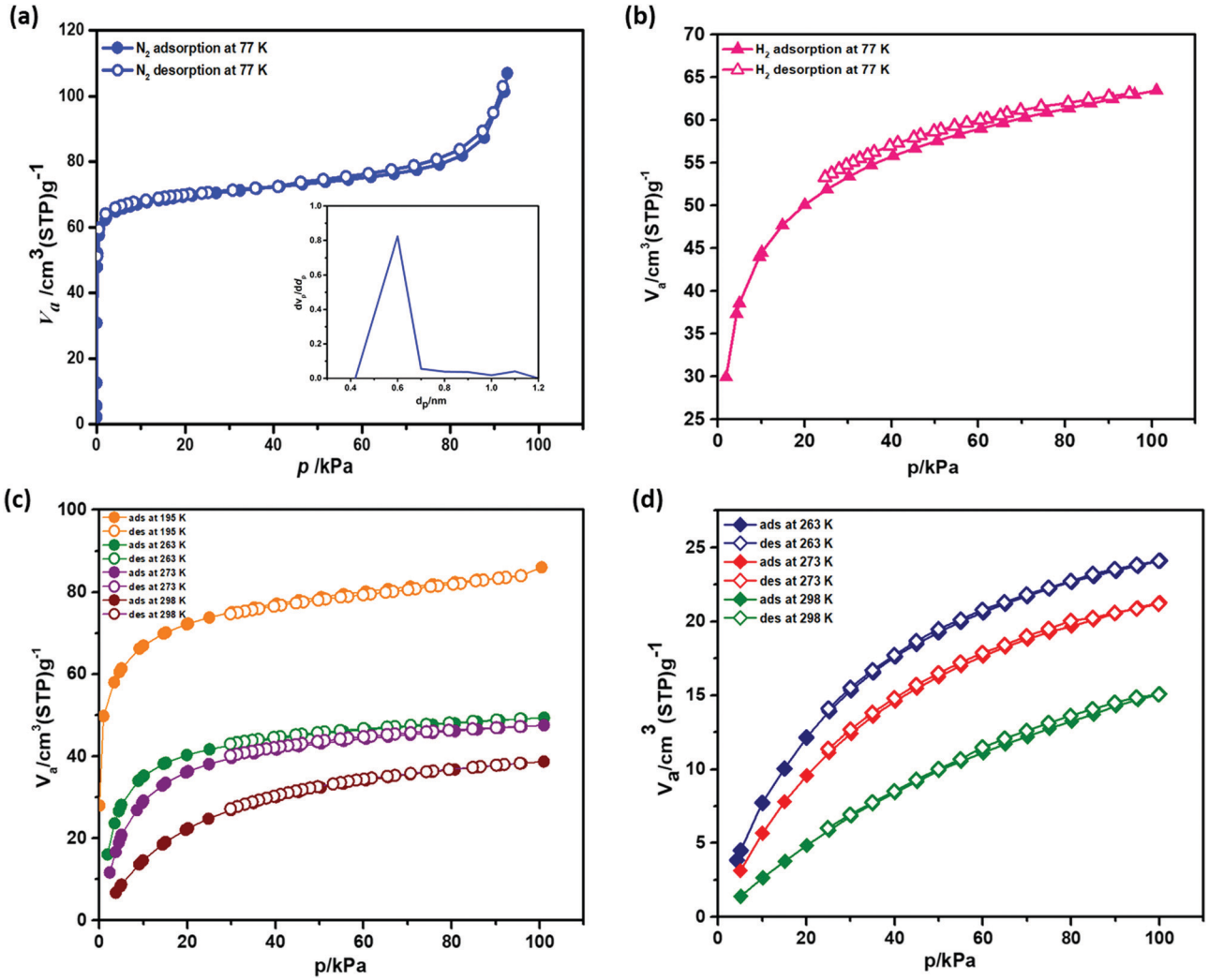

Fig. 4 Gas sorption of **Zn-CBS**: (a) N_2 sorption isotherm and pore size distribution; (b) H_2 sorption isotherm at 77 K; (c) CO_2 sorption isotherms at 195 K, 263 K, 273 K, and 298 K; (d) CH_4 sorption isotherms at 263 K, 273 K and 298 K.

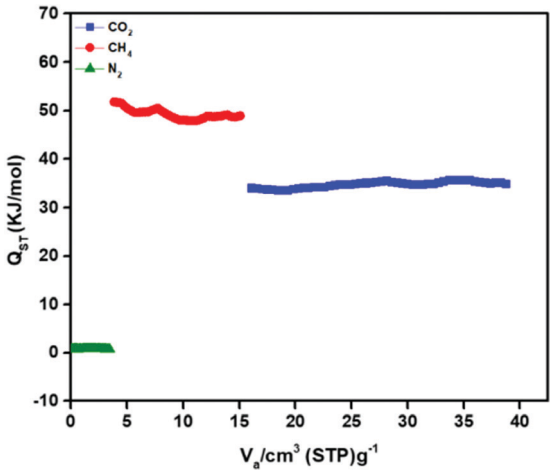

Fig. 5 Isosteric heat of adsorption (Q_{st}) for CO_2, CH_4 and N_2 using experimental isotherm data of **Zn-CBS** at 263 K, 273 K and 298 K.

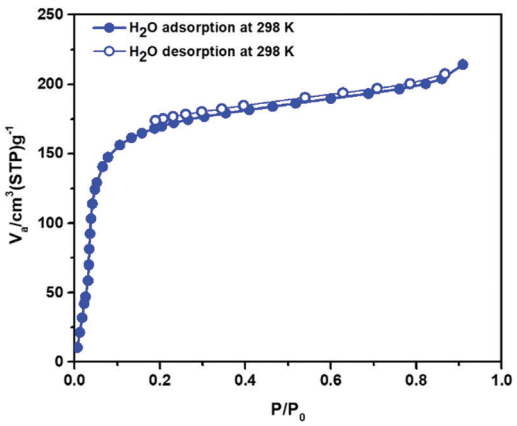

Fig. 6 Water adsorption–desorption isotherm of **Zn-CBS**.

saturation plateau that are usually found for zeolites is remarkable. This type of materials which show more adsorption of the adsorbate at lower P/P_0, can be good candidate as a desiccant.[49] At higher P/P_0 value (0.8–1.0), it shows an uptake of $\sim$221 cm^3 (STP) g^{-1} (Fig. 6), amounting to seven water molecules per formula unit. As indicated in the thermal analysis section and later utilized such property for solvent encapsulation, the framework is stable upon loss of lattice water molecules and has a permanent pore. This sorption study validates the hydrophilic interaction between the framework and the water molecules. The PXRD of the used **Zn-CBS** was recorded after the gas and vapor adsorption experiments (Fig. S12, ESI†). It shows that the crystallinity and structural integrity of the framework are maintained. Interestingly, there are only few MOFs which show such permanent porosity.[17] On the other hand, examples of amino acid-based MOFs demonstrating both CO_2 and water sorption are rare.

Selectivity of CO_2/N_2 and CO_2/CH_4 by IAST method

The potential for gas separation by **Zn-CBS** was investigated by using ideal adsorbed solution theory (IAST) method (see ESI,† for details). The dual-site Langmuir–Freundlich (DSLF)

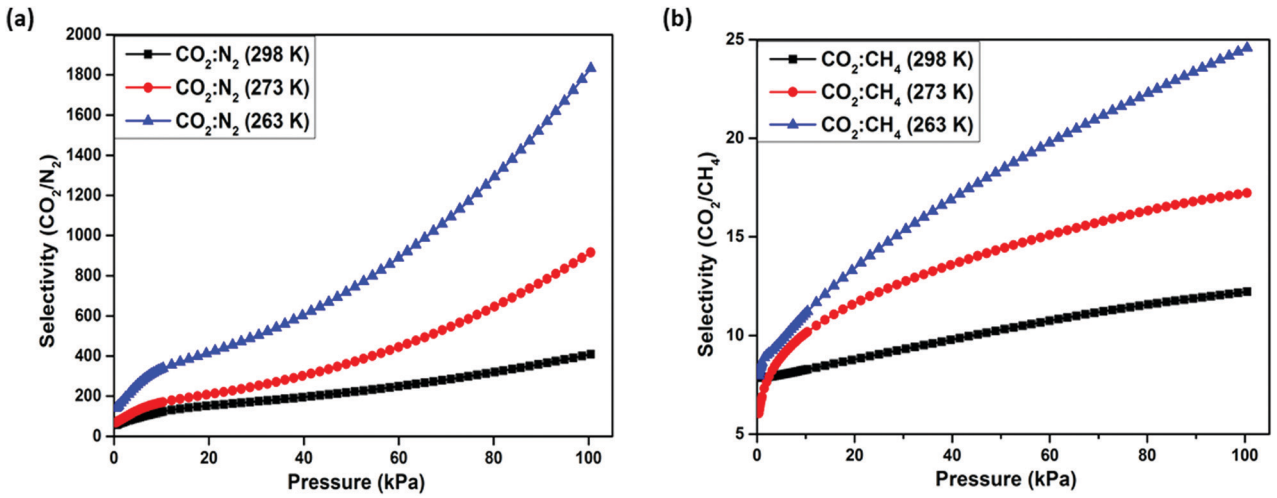

Fig. 7 Separation selectivity of **Zn-CBS** at 263 K, 273 K, and 298 K predicted by IAST for (a) CO_2/N_2 (15/85); and (b) CO_2/CH_4 (50/50).

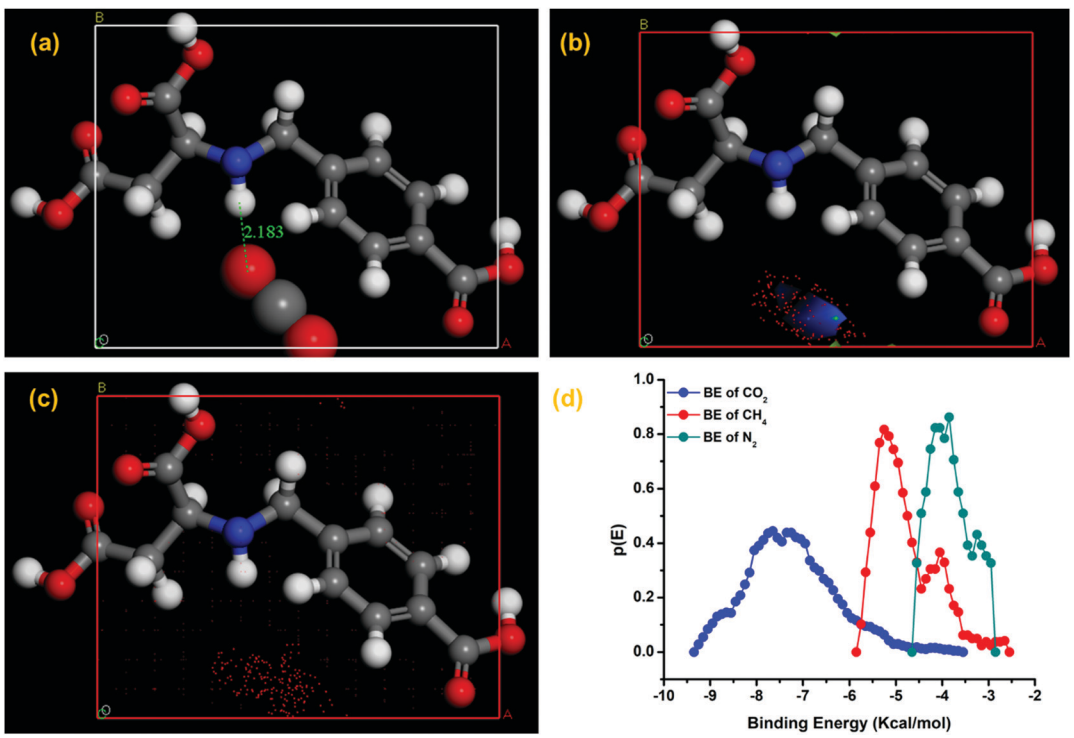

Fig. 8 CBMC simulation: (a) interaction and distance between CO_2 molecules and H_3(D-2,4-cbs) present as a trianion in **Zn-CBS** at 298 K; probability density of (b) CH_4 and (c) N_2 at 298 K; (d) binding energy of CO_2, CH_4, and N_2.

isotherm model has been utilized for fitting the unary isotherm of three gases, *i.e.*, CO_2, N_2 and CH_4 at three different temperatures 263 K, 273 K and 298 K, respectively (Table S2 and Fig. S13–S21, ESI†). The selectivity values for CO_2/N_2 (15 : 85, flue gas composition) and CO_2/CH_4 (50 : 50, landfill gas composition) are measured using this equation. The calculated selectivity for CO_2/N_2 (15 : 85) mixture is 1832, 916 and 408 at 298 K, 273 K and 263 K, respectively (Fig. 7a). On the other hand, the selectivity of CO_2/CH_4 (50 : 50) mixture is 24.5, 17.2 and 12.2 at 298 K, 273 K and 263 K, respectively (Fig. 7b). The selectivity of CO_2/N_2 and CO_2/CH_4 is higher than the MOFs reported in Table S3 (ESI†).[14–16,24,50–52] The high selectivity of CO_2 over CH_4 and N_2 may be accredited to the presence of an amine group in the framework.

To better understand the high selectivity of CO_2 over CH_4 and N_2, configurational bias Monte Carlo (CBMC) simulation using BIOVIA, Material studio 2007 was carried out.[53] The amine basic site in the H_3(D-2,4-cbs) ligand, which is present as a trianion in **Zn-CBS**, plays a crucial role in high selectivity. For this purpose H_3(D-2,4-cbs) was taken into account, optimized in Density Functional Theory (DFT) and put in a (1 × 1 × 1) cell. Using the sorption module, with respect to the ligand the position of different gases and their binding energy (BE) at 298 K with a fixed pressure of 1 bar have been determined. It is observed that only one CO_2 molecule was adsorbed and the intermolecular distance between CO_2 and the N–H moiety of the ligand was found to be 2.18 Å (N–H···O) and the bond angle of CO_2 is reduced to 174.9° (Fig. 8a). On the other hand, N_2 and CH_4 do not show any interaction but some electron density was observed near the N–H bond of the ligand (Fig. 8b and c). The probable electron density of CH_4 was almost triple compared to N_2. The BE of CO_2 (−7.45 kcal mol^{-1}) is higher than that of N_2 (−4.4 kcal mol^{-1}) and CH_4 (−5.5 kcal mol^{-1}), confirming the high sorption and selectivity (Fig. 8d).

Encapsulation of solvent molecules and chemical stability

Based on the porosity of **Zn-CBS** confirmed by nitrogen gas and water vapor sorption studies, the encapsulation of various organic solvents, like acetonitrile, ethanol, methanol, tetrahydrofuran, toluene, and *p*-xylene, inside the MOF was carried out by activating it at 100 °C for 3 h under high vacuum. Experiments were performed by soaking the activated **Zn-CBS** in different organic solvents for 3 days, where the respective fresh solvent was used after every 24 h, and dried in air. In order to understand the framework stability and get an estimate of

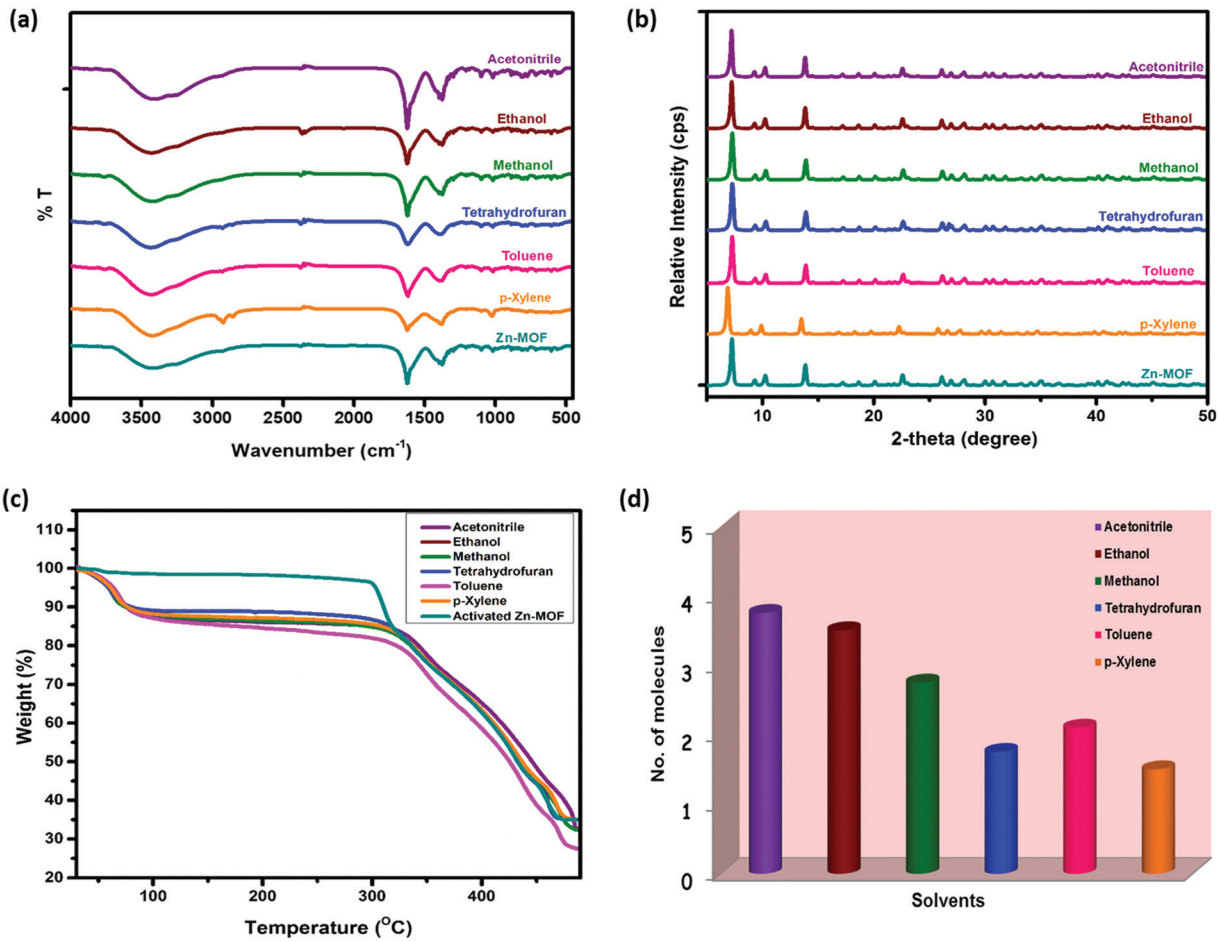

Fig. 9 Encapsulation of solvents by **Zn-CBS**: (a) comparison of FTIR spectra; (b) PXRD patterns; (c) TG profiles after encapsulation of various organic solvents; and (d) bar plot representing the total number of solvent molecules encapsulated per formula unit of the framework.

solvent absorbed by **Zn-CBS**, the solvated framework was examined by FTIR, PXRD, and TGA. The FTIR spectra (Fig. 9a) confirm the stability of the framework in the encapsulated solvents. Further, PXRD indicates that crystallinity and structural integrity of the framework are maintained after the encapsulation of different solvents (Fig. 9b). From the TG profiles of encapsulated **Zn-CBS** with various solvents compared to its activated form, the stability of the framework after the loss of solvent is intact (Fig. 9c). The number of solvent molecules encapsulated by the framework is calculated (Table S4, ESI†) and depicted in Fig. 9d. Based on this information, it is clear that the maximum absorbing capacity of **Zn-CBS** is for acetonitrile as it has the highest dipole moment and is linear in shape. The remarkable encapsulation of different solvents can be attributed to the interaction of the solvent with a framework depending on the size and polarity of the solvent.

Conclusion

A homochiral Zn(II)-organic nanoflower, **Zn-CBS**, was solvothermally synthesized using a new amino acid-based tricarboxylate ligand. Both FESEM and TEM images showed details of the nanoflower arrangement in **Zn-CBS**. Based on the N_2 adsorption measurements (reversible type I isotherm) the microporous nature of the framework was established. The amine functionality present in the micropore wall helped to capture more CO_2 over N_2 and CH_4 because of strong adsorbate-adsorbent interaction. However, the Q_{st} value for CH_4 (51.8 kJ mol^{-1}) is higher than that for CO_2 (35 kJ mol^{-1}) because of appropriate pore size of the framework. The high selectivity of CO_2 over CH_4 and N_2 shows its potential under relevant flue and landfill gas separation conditions. On the other hand, water sorption isotherm showed high water uptake (156 cm^3 (STP) g^{-1}) at lower relative pressure, indicating a strong interaction between framework and polar molecules for a potential desiccant use. The porosity of the framework was further utilized for encapsulating small molecules such as various common solvents, which was monitored by FTIR, TGA and PXRD analysis. These gas and vapour sorption studies substantiate the permanent microporosity of **Zn-CBS**. Thus, with high thermal and water stability **Zn-CBS** is a versatile material that is suitable for selective CO_2 capture and separation, and encapsulating solvent molecules. Extension of this work with different ligand systems for generating new MOFs containing larger micropores with various applications is currently underway in our laboratory.

Conflicts of interest

There are no conflicts to declare.

Acknowledgements

Funding for this work was provided by IISER, Mohali. S. G. is grateful to UGC and P. D. is grateful to MHRD, India for research fellowships. The use of NMR, X-ray, SAXS, CHN, FESEM and other departmental facilities at IISER Mohali; and HRTEM facility at NIPER Mohali is gratefully acknowledged.

References

1 (*a*) S. S. Han, J. L. Mendoza-Cortés and W. A. Goddard III, *Chem. Soc. Rev.*, 2009, **38**, 1460–1476; (*b*) L. J. Murray, M. Dincă and J. R. Long, *Chem. Soc. Rev.*, 2009, **38**, 1294–1314; (*c*) Y. Salinas, R. Martínez-Máñez, M. D. Marcos, F. Sancenón, A. M. Costero, M. Parra and S. Gil, *Chem. Soc. Rev.*, 2012, **41**, 1261–1296; (*d*) S. Letzel, T. Göen, M. Bader, J. Angerer and T. Kraus, *Occup. Environ. Med.*, 2003, **60**, 483–488.

2 (*a*) A. Corma, H. García and F. X. LlabrésiXamena, *Chem. Rev.*, 2010, **110**, 4606–4655; (*b*) J. Lee, O. K. Farha, J. Roberts, K. A. Scheidt, S. T. Nguyen and J. T. Hupp, *Chem. Soc. Rev.*, 2009, **38**, 1450–1459; (*c*) E. B. Bauer, *Chem. Soc. Rev.*, 2012, **41**, 3153–3167; (*d*) C. N. R. Rao, S. S. Natarajan and R. Vaidhyanathan, *Angew. Chem. Int. Ed.*, 2004, **43**, 1466–1496.

3 B. Li, Z. Zhang, Y. Li, K. Yao, Y. Zhu, Z. Deng, F. Yang, X. Zhou, G. Li, H. Wu, N. Nijem, Y. J. Chabal, Z. Lai, Y. Han, Z. Shi, S. Feng and J. Li, *Angew. Chem., Int. Ed.*, 2012, **51**, 1412–1415.

4 K. Sumida, D. L. Rogow, J. A. Mason, T. M. McDonald, E. D. Bloch, Z. R. Herm, T.-H. Bae and J. R. Long, *Chem. Rev.*, 2012, **112**, 724–781.

5 Z.-R. Qu, H. Zhao, X.-S. Wang, Y.-H. Li, Y.-M. Song, Y.-J. Liu, Q. Ye, R.-G. Xiong, B. F. Abrahams, Z.-L. Xue and X.-Z. You, *Inorg. Chem.*, 2003, **42**, 7710–7712.

6 J.-R. Li, R. J. Kuppler and H.-C. Zhou, *Chem. Soc. Rev.*, 2009, **38**, 1477–1504.

7 K. Sumida, D. L. Rogow, J. A. Mason, T. M. McDonald, E. D. Bloch, Z. R. Herm, T.-H. Bae and J. R. Long, *Chem. Rev.*, 2012, **112**, 724–781.

8 T. M. McDonald, J. A. Mason, X. Kong, E. D. Bloch, D. Gygi, A. Dani, V. Crocella, F. Giordanino, S. O. Odoh, W. S. Drisdell, B. Vlaisavljevich, A. L. Dzubak, R. Poloni, S. K. Schnell, N. Planas, K. Lee, T. Pascal, L. F. Wan, D. Prendergast, J. B. Neaton, B. Smit, J. B. Kortright, L. Gagliardi, S. Bordiga, J. A. Reimer and J. R. Long, *Nature*, 2015, **519**, 303–308.

9 M. Carta, R. Malpass-Evans, M. Croad, Y. Rogan, J. C. Jansen, P. Bernardo, F. Bazzarelli and N. B. McKeown, *Science*, 2013, **339**, 303–307.

10 G. Feng, Y. Peng, W. Liu, F. Chang, Y. Dai and W. Huang, *Inorg. Chem.*, 2017, **56**, 2363–2366.

11 B. Zheng, J. Bai, J. Duan, L. Wojtas and M. J. Zaworotko, *J. Am. Chem. Soc.*, 2011, **133**, 748–751.

12 S. Nandi, R. Maity, D. Chakraborty, H. Ballav and R. Vaidhyanathan, *Inorg. Chem.*, 2018, **57**, 5267–5272.

13 (*a*) J. Liu, P. K. Thallapally, B. P. McGrail, D. R. Brown and J. Liu, *Chem. Soc. Rev.*, 2012, **41**, 2308–2322; (*b*) H. Wang, Q.-L. Zhu, R. Zou and Q. Xu, *Nat. Energy*, 2016, **1**, 16034–16046.

14 Q. G. Zhai, Q. P. Lin, T. Wu, L. Wang, S. T. Zheng, X. Bu and P. Feng, *Chem. Mater.*, 2012, **24**, 2624–2626.

15 A. Pal, S. Chand, S. M. Elahi and M. C. Das, *Dalton Trans.*, 2017, **46**, 15280–15286.

16 R. B. Lin, D. Chen, Y. Y. Lin, J. P. Zhang and X. M. Chen, *Inorg. Chem.*, 2012, **51**, 9950–9955.

17 (*a*) C. Janiak, *Chem. Commun.*, 2013, **49**, 6933–6937; (*b*) L. Feng, K. Y. Wang, J. Willman and H. C. Zhou, *ACS Cent. Sci.*, 2020, **6**, 359–367.

18 C. M. Gastaldo, J. E. Warren, M. E. Briggs, J. A. Armstrong, K. M. Thomas and M. J. Rosseinsky, *Chem. – Eur. J.*, 2015, **21**, 16027–16034.
19 P. Das and S. K. Mandal, *ACS Appl. Mater. Interfaces*, 2018, **10**, 25360–25371.
20 S. Bourrelly, P. L. Llewellyn, C. Serre, F. Millange, T. Loiseau and G. Férey, *J. Am. Chem. Soc.*, 2005, **127**, 13519–13521.
21 A. Kansari, M. R. Bryant, D. R. Jenkinson, G. B. Jameson, O. T. Qazvini, L. Liu, A. D. Burrows, S. G. Telfer and C. Richardson, *CrystEngComm*, 2019, **21**, 7498–7506.
22 J. An and N. L. Rosi, *J. Am. Chem. Soc.*, 2010, **132**, 5578–5579.
23 Z. Liang, M. Marshall and A. L. Chaffee, *Microporous Mesoporous Mater.*, 2010, **132**, 305–310.
24 S. Yang, X. Lin, W. Lewis, M. Suyetin, E. Bichoutskaia, J. E. Parker, C. C. Tang, D. R. Allan, P. R. Rizkallah, P. Hubberstey, N. R. Champness, K. M. Thomas, A. J. Blake and M. Schroder, *Nat. Mater.*, 2012, **11**, 710–716.
25 Z. Zhang, S. Xiang, X. Rao, Q. Zheng, F. R. Fronczek, G. Qian and B. Chen, *Chem. Commun.*, 2010, **46**, 7205–7207.
26 D. Farrusseng, C. Daniel, C. Gaudillere, U. Ravon, Y. Schuurman, C. Mirodatos, D. Dubbeldam, H. Frost and R. Q. Snurr, *Langmuir*, 2009, **25**, 7383–7388.
27 L. Kong, R. Zou, W. Bi, R. Zhong, W. Mu, J. Liu, R. P. S. Hana and R. Zou, *J. Mater. Chem. A*, 2014, **2**, 17771–17778.
28 M. H. Choi, H. J. Park, D. H. Hong and M. P. Suh, *Chem. – Eur. J.*, 2013, **19**, 17432–17438.
29 A. Pal, S. Chand and M. C. Das, *Inorg. Chem.*, 2017, **56**, 13991–13997.
30 (*a*) N. Zhao, F. Sun, P. Li, X. Mu and G. Zhu, *Inorg. Chem.*, 2017, **56**, 6938–6942; (*b*) L. Ma, J. Y. Lee, J. Li and W. Lin, *Inorg. Chem.*, 2008, **47**, 3955–3957; (*c*) S. K. Das, S. Chatterjee, S. Bhunia, A. Mondal, P. Mitra, V. Kumari, A. Pradhan and A. Bhaumik, *Dalton Trans.*, 2017, **46**, 13783–13792.
31 E. Stavitski, E. A. Pidko, S. Couck, T. Remy, E. J. M. Hensen, B. M. Weckhuysen, J. Denayer, J. Gascon and F. Kapteijn, *Langmuir*, 2011, **27**, 3970–3976.
32 Y. Zhao, H. Wu, T. J. Emge, Q. Gong, N. Nijem, Y. J. Chabal, L. Kong, D. C. Langreth, H. Liu, H. Zeng and J. Li, *Chem. – Eur. J.*, 2011, **17**, 5101–5109.
33 H.-P. Li, S.-N. Li, H.-M. Sun, M.-C. Hu, Y.-C. Jiang and Q.-G. Zhai, *Cryst. Growth Des.*, 2018, **18**, 3229–3235.
34 T. Panda, P. Pachfule, Y. Chen, J. Jiang and R. Banerjee, *Chem. Commun.*, 2011, **47**, 2011–2013.
35 J.-P. Zhang, A.-X. Zhu, R.-B. Lin, X.-L. Qi and X.-M. Chen, *Adv. Mater.*, 2011, **23**, 1268–1271.
36 J.-P. Lin, J.-P. Zhang and X.-M. Chen, *J. Am. Chem. Soc.*, 2010, **132**, 6654–6656.
37 A. Phan, C. J. Doonan, F. J. Uribe-Romo, C. B. Knobler, M. O'Keeffe and O. M. Yaghi, *Acc. Chem. Res.*, 2010, **43**, 58–67.
38 (*a*) H. Li, M. Eddaoudi, M. O'Keeffe and O. M. Yaghi, *Nature*, 1999, **402**, 276–278; (*b*) H. K. Chae, J. Kim, O. D. Friedrichs, M. O'Keeffe and O. M. Yaghi, *Angew. Chem., Int. Ed.*, 2003, **42**, 3907–3909; (*c*) H. K. Chae, D. Y. Siberio-Perez, J. Kim, Y. Go, M. Eddaoudi, A. J. Matzger, M. O'Keeffe and O. M. Yaghi, *Nature*, 2004, **427**, 523–526; (*d*) L. K. Macreadie, E. J. Mensforth, R. Babarao, K. Konstas, S. G. Telfer, C. M. Doherty, J. Tsanaktsidis, S. R. Batten and M. R. Hill, *J. Am. Chem. Soc.*, 2019, **141**, 3828–3832; (*e*) X. Zhao, H. Yang, E. T. Nguyen, J. Padilla, X. Chen, P. Feng and X. Bu, *J. Am. Chem. Soc.*, 2018, **140**, 13566–13569; (*f*) X. Lou, F. Geng, B. Hu, C. Li, M. Shen and B. Hu, *ACS Appl. Energy Mater.*, 2019, **2**, 413–419; (*g*) D. Wu, J. Liu, J. Jin, J. Cheng, M. Wang, G. Yang and Y.-Y. Wang, *Cryst. Growth Des.*, 2019, **19**, 6774–6783; (*h*) C. Zhuo, Y. Wen and X. Wu, *CrystEngComm*, 2016, **18**, 2792–2902.
39 (*a*) Y.-X. Ren, S.-S. Xiao, X.-J. Zheng, L.-C. Li and L.-P. Jina, *Dalton Trans.*, 2012, **41**, 2639–2647; (*b*) B. An, R. Zhou, D. Dang, J. Wang, H. Pan and Y. Bai, *Spectrochim. Acta, Part A*, 2014, **122**, 392–399; (*c*) J. Tao, X. Yin, Z. B. Wei, R. B. Huang and L. S. Zheng, *Eur. J. Inorg. Chem.*, 2004, 125–133; (*d*) N. Wang, J. G. Ma, W. Shi and P. Cheng, *Cryst. Eng. Commun.*, 2012, **14**, 5634–5638; (*e*) J. Tao, M.-L. Tong, J.-X. Shi, X.-M. Chen and S. W. Ngb, *Chem. Commun.*, 2000, 2043–2044; (*f*) B. Bhattacharya, D. Saha, D. K. Maity, R. Dey and D. Ghoshal, *Cryst. Eng. Commun.*, 2014, **16**, 4783–4795; (*g*) S. Khan, P. Das and S. K. Mandal, *Inorg. Chem.*, 2020, **59**, 4588–4600.
40 X. Lv, L. Li, S. Tang, C. Wang and X. Zhao, *Chem. Commun.*, 2014, **50**, 6886–6889.
41 C. Wang, D. Liu and W. Lin, *J. Am. Chem. Soc.*, 2013, **135**, 13222–13234.
42 R. Saha, B. Joarder, A. S. Roy, Sk. M. Islam and S. Kumar, *Chem. – Eur. J.*, 2013, **19**, 16607–16614.
43 (*a*) R. W. Flag, M. O. Popp, A. M. Fracaroli, E. A. Kapustin, M. J. Kalmutzki, R. M. Altamimi, F. Fathieh, J. A. Reimer and O. M. Yaghi, *J. Am. Chem. Soc.*, 2017, **139**, 12125–12128; (*b*) F.-Y. Yi, S.-C. Wang, M. Gu, J.-Q. Zheng and L. Han, *J. Mater. Chem. C*, 2018, **6**, 2010–2018.
44 C. Zhuo, Y. Wen and X. Wu, *Cryst. Eng. Commun.*, 2016, **18**, 2792–2802.
45 (*a*) S. Ma, X. S. Wang, C. D. Collier, E. S. Manis and H. C. Zhou, *Inorg. Chem.*, 2007, **46**, 8499–8501; (*b*) D. Chandra, M. W. Kasture and A. Bhaumik, *Microporous Mesoporous Mater.*, 2008, **116**, 204–209.
46 O. K. Farha, K. L. Mulfort and J. T. Hupp, *Inorg. Chem.*, 2008, **47**, 10223–10225.
47 K. Nakamoto, *Infrared and Raman Spectra of Inorganic and Coordination Compounds: Part B: Applications in Coordination, Organometallic, and Bioinorganic Chemistry*, John Wiley & Sons, Inc., Hoboken, NJ, 6th edn, 2008.
48 D. Bradshaw, J. B. Claridge, E. J. Cussen, T. J. Prior and M. J. Rosseinsky, *Acc. Chem. Res.*, 2005, **38**, 273–282.
49 X. Zheng, T. S. Ge and R. Z. Wang, *Energy*, 2014, **74**, 280–294.
50 S. Xiong, Y. Gong, H. Wang, Q. Liu, M. Gu, X. Wang, B. Chen and Z. Wang, *Chem. Commun.*, 2014, **50**, 12101–12104.
51 Z.-J. Lin, Y.-B. Huang, T.-F. Liu, X.-Y. Li and R. Cao, *Inorg. Chem.*, 2013, **52**, 3127–3132.
52 S. Xiang, Y. He, Z. Zhang, H. Wu, W. Zhou, R. Krishna and B. Chen, *Nat. Commun.*, 2012, **3**, 954–963.
53 S. Yeganegi, M. Gholami and V. Sokhanvaran, *Mol. Simul.*, 2017, **43**, 260–266.